$(C_5H_9NH_3)_2CuBr_4$: a metal-organic two-ladder quantum magnet

J. Philippe,[1,2,*] F. Elson,[3] N. P. M. Casati,[4,†] S. Sanz,[5] M. Metzelaars,[5,6] O. Shliakhtun,[1,2] O. K. Forslund,[2,7] J. Lass,[8,9] T. Shiroka,[10] A. Linden,[11] D. G. Mazzone,[8] J. Ollivier,[12] S. Shin,[13] M. Medarde,[13] B. Lake,[14,15] M. Månsson,[3] M. Bartkowiak,[1] B. Normand,[16,17] P. Kögerler,[6] Y. Sassa,[18] M. Janoschek,[1,2] and G. Simutis[1,18,‡]

[1]*Laboratory for Neutron and Muon Instrumentation, Paul Scherrer Institut, CH-5232 Villigen-PSI, Switzerland*
[2]*Physik-Institut, Universität Zürich, Winterthurerstrasse 190, CH-8057 Zürich, Switzerland*
[3]*Department of Applied Physics, KTH Royal Institute of Technology, SE-106 91 Stockholm, Sweden*
[4]*Swiss Light Source, Paul Scherrer Institut, CH-5232 Villigen-PSI, Switzerland*
[5]*Peter Grünberg Institute, Electronic Properties (PGI-6), Forschungszentrum Jülich, 52425 Jülich, Germany*
[6]*Institute of Inorganic Chemistry, RWTH Aachen University, 52056 Aachen, Germany*
[7]*Department of Physics and Astronomy, Uppsala University, Box 516, SE-75120 Uppsala, Sweden*
[8]*Laboratory for Neutron Scattering and Imaging, Paul Scherrer Institut, CH-5232 Villigen-PSI, Switzerland*
[9]*Laboratory for Quantum Magnetism, Ecole Polytechnique Fédérale de Lausanne (EPFL), CH-1015 Lausanne, Switzerland*
[10]*Laboratory for Muon Spin Spectroscopy, Paul Scherrer Institut, CH-5232 Villigen-PSI, Switzerland*
[11]*Chemistry Department, University of Zurich, Winterthurerstrasse 190, CH-8057 Zürich, Switzerland*
[12]*Institut Laue Langevin, BP156, 38042 Grenoble, France*
[13]*Laboratory for Multiscale Materials Experiments, Paul Scherrer Institut, CH-5232 Villigen-PSI, Switzerland*
[14]*Helmholtz-Zentrum Berlin für Materialien und Energie, Hahn-Meitner-Platz 1, 14109 Berlin, Germany*
[15]*Institut für Festkörperforschung, Technische Universität Berlin, 10623 Berlin, Germany*
[16]*Laboratory for Theoretical and Computational Physics, Paul Scherrer Institut, CH-5232 Villigen-PSI, Switzerland*
[17]*Institute of Physics, Ecole Polytechnique Fédérale de Lausanne (EPFL), CH-1015 Lausanne, Switzerland*
[18]*Department of Physics, Chalmers University of Technology, SE-41296 Göteborg, Sweden*

(Dated: April 15, 2024)

Low-dimensional quantum magnets are a versatile materials platform for studying the emergent many-body physics and collective excitations that can arise even in systems with only short-range interactions. Understanding their low-temperature structure and spin Hamiltonian is key to explaining their magnetic properties, including unconventional quantum phases, phase transitions, and excited states. We study the metal–organic coordination compound $(C_5H_9NH_3)_2CuBr_4$ and its deuterated counterpart, which upon its discovery was identified as a candidate two-leg quantum ($S = 1/2$) spin ladder in the strong-leg coupling regime. By growing large single crystals and probing them with both bulk and microscopic techniques, we deduce that two previously unknown structural phase transitions take place between 136 K and 113 K. The low-temperature structure has a monoclinic unit cell giving rise to two inequivalent spin ladders. We further confirm the absence of long-range magnetic order down to 30 mK and discuss the implications of this two-ladder structure for the magnetic properties of $(C_5H_9NH_3)_2CuBr_4$.

I. INTRODUCTION

One-dimensional quantum magnets provide a testbed for many-body quantum physics, because experimental measurements of their intrinsically collective excitations can be described by powerful analytical and numerical techniques. One particularly versatile model system is the two-leg $S = 1/2$ quantum spin ladder, which with isotropic (Heisenberg) interactions is described by only two parameters, $J_{\rm leg}$ for the ladder legs and $J_{\rm rung}$ for the rungs, and hence by a single ratio, $\alpha = J_{\rm leg}/J_{\rm rung}$ [1]. Although these ladders have a spin gap for any finite α and can all be described in a resonating valence-bond framework with different correlation distributions [2], the zero-field spectral function varies widely from a single triplon branch in strong-rung ladders ($\alpha < 1/2$) to weakly confined spinons in the spin-chain limit ($\alpha \gg 1$) [3].

Arguably the most interesting properties of two-leg ladders appear in an applied magnetic field strong enough to close the spin gap, where the system becomes a spin Tomonaga–Luttinger liquid (TLL), a theoretical model describing interacting fermions in one dimension [4]. Early ladder materials, based on cuprate perovskites, included $SrCu_2O_3$ [5–8], $LaCuO_{2.5}$ [9], and $(Sr_{14-x}Ca_x)Cu_{24}O_{41}$ [10, 11]; these systems had $\alpha \approx 1$ with $J_{\rm leg}$ and $J_{\rm rung}$ both very large, and thus far outside the range of laboratory magnetic fields. Metal-organic materials based on Cu^{2+} ions offered a solution to producing low-J ladders, and much of the TLL phenomenology was discovered using the strong-rung system $(C_5H_{12}N)_2CuBr_4$ (BPCB) [12, 13], including triplon fractionalization [14], three-dimensional ordering [15], and the full spectral function of all three field-split triplon branches [16]. Two-leg ladders have also been used as a platform for observing two-triplon bound states in the absence of frustration [17–19] and, in the presence of strong frustration, for the theoretical study of fully localized quasiparticles, exact bound states, and anomalous thermodynamics [20–22].

Materials in the strong-leg regime, $\alpha > 1$, nevertheless retain a special interest due to the delocalized and spinonic character of their correlations and excitations. To date $(C_7H_{10}N_2)_2CuBr_4$ (DIMPY) is the only clean, strong-leg ladder compound to be studied in detail, with extensive bulk and spectroscopic studies performed to unravel its magnetic properties [3, 18, 23–26]. In the

* jonas.philippe@psi.ch
† nicola.casati@psi.ch
‡ gediminas.simutis@psi.ch

TLL, it was shown that the interaction between the emergent fermions depends both on α and on the applied field, such that in DIMPY it could be controlled and made attractive by increasing the field [27–30]. In the direction of controlled disorder physics, it was found when depleted by spinless impurities that the ladders in DIMPY host emergent strongly interacting spin islands [31].

Despite this level of understanding, DIMPY has also been found to exhibit field-induced low-temperature phases that are not expected for the ideal two-leg ladder [32], pointing to the presence of additional terms in the spin Hamiltonian. Theoretical studies have shown that readily anticipated extra terms, such as Dzyaloshinskii-Moriya (DM) interactions and frustration, have substantial effects on the properties and phase diagram [33–35]. For this reason, additional materials of the strong-leg ladder type are required to separate universal from non-universal properties. Further, given the change in ladder nature as a function of α, additional materials spanning the full α range are required for detailed experimental analysis of the crossover from triplonic to spinonic physics in quantum spin ladders.

To expand the platform of model materials, in this paper we investigate $(C_5H_9NH_3)_2CuBr_4$ and its deuterated counterpart, $(C_5D_9ND_3)_2CuBr_4$, to both of which we refer as Cu-CPA. Upon its discovery, this compound was proposed as a candidate strong-leg spin ladder with $\alpha = 2.11$ [36]. At room temperature, Cu-CPA has an orthorhombic structure in which the Cu^{2+} ions are linked by halogen (Br$\cdots$Br) bonds to form a structure of well-isolated magnetic motifs separated by organic cations. At $T_{2a} = 260$ K, the authors of Ref. [36] found a structural phase transition accompanied by a doubling of the crystallographic a axis, with the unit cell remaining orthorhombic.

We have performed diffraction measurements at 203 K that confirm this structure, which is shown in Fig. 1(b). The bond lengths and magnetic interaction pathways suggest that Cu-CPA should realize a strong-leg ladder, with any further-neighbor interactions, which include diagonal and interladder pathways, being negligible. Initial magnetic susceptibility measurements support this scenario, but are far from conclusive. More detailed studies of Cu-CPA have, however, been hampered by the difficulty in producing sizeable single crystals. Here we overcome this challenge by optimizing the crystal growth from solution and thus obtaining large single crystals of both hydrogenated and deuterated Cu-CPA.

Our detailed structural and thermodynamic measurements reveal that the low-temperature structure of Cu-CPA is significantly richer than the initial studies suggested. In particular, the system undergoes two more structural phase transitions below T_{2a}, which take it into a low-temperature monoclinic phase. Using neutron and X-ray diffraction, we establish that at low temperatures Cu-CPA contains two structurally inequivalent ladders, as shown in Fig. 1(a).

This paper is organized as follows. In Sec. II we describe the materials and methods used in our study. We present our experimental results for the presence of two inequivalent ladders in Sec. III. In Sec. IV we discuss the implications of this situation for the magnetic properties of Cu-CPA and in Sec. V we provide a brief conclusion.

II. MATERIALS AND METHODS

A. Crystal Growth

The single crystals of Cu-CPA used for this study were synthesized using growth from solution. The synthesis method reported earlier [36] was optimized to produce large single crystals. Deuterated versions of the compound were produced in the same manner, in order to make possible high-resolution neutron scattering experiments.

We focus our description on the synthesis of $(C_5D_9ND_3)_2CuBr_4$. First, a 47 weight % DBr solution in D_2O (18.20 ml, 0.129 mol) was added dropwise to a solution of cyclopentylamine-d_{11} (11.25 g, 0.117 mol) in 20 ml of D_2O. The resulting mixture was stirred for five minutes and left to stand for slow evaporation in the fume hood until white crystals appeared. Crystals of cyclopentylammonium bromide-d_{12} (CPA-DBr) were filtered and dried in vacuum for five hours. Subsequently, CPA-DBr (0.88 g, 5 mmol) was dissolved in 6 ml of D_2O and, to this mixture, a solution of $CuBr_2$ (0.56 g, 2.50 mmol) in 10 ml of D_2O was added dropwise and stirred for five minutes. To this final solution, 2 ml of 48% DBr in D_2O was added dropwise to avoid hydrolysis [formation of $Cu(OD)_2$]. The solution was filtered and left to stand in a beaker for slow evaporation. After three months, long black needles (of approximate size $20 \times 2 \times 2$ mm) grew as single crystals in the mother solution.

B. Characterization

The specific heat was measured at zero field (ZF) and in an applied magnetic field of $\mu_0 H = 7$ T in a Quantum Design Physical Property Measurement System (PPMS) for the respective temperature ranges 4–200 K and 80–160 K. Low-temperature measurements over the range 0.36–20 K were performed, using a Quantum Design ^{3}He insert for the PPMS, to provide sufficient overlap with the conventional ^{4}He measurements. The standard ZF measurements were performed on a twinned, deuterated Cu-CPA crystal [mass 7.00(1) mg] and repeated with a deuterated, single crystal of mass 1.34(1) mg. The measurements in field were performed on the same single crystal [mass 1.34(1) mg] used for the standard ZF measurements. The ^{3}He measurements were performed on a different deuterated single crystal, also of mass 1.34(1) mg. Finally, the ZF measurements (over temperature range 4–200 K) on hydrogenated Cu-CPA were performed on a single crystal of mass 1.10(1) mg.

C. X-ray diffraction measurements

Single-crystal X-ray diffraction measurements were performed with a Stadivari diffractometer (STOE) equipped with a liquid-nitrogen open-flow cooler (Oxford Cryosystems, Cryostream) that enabled the acquisition of X-ray diffraction data down to 85 K. Monochromated Mo Kα radiation was used and full structural datasets were acquired at 85, 125, and 203 K, while further, partial

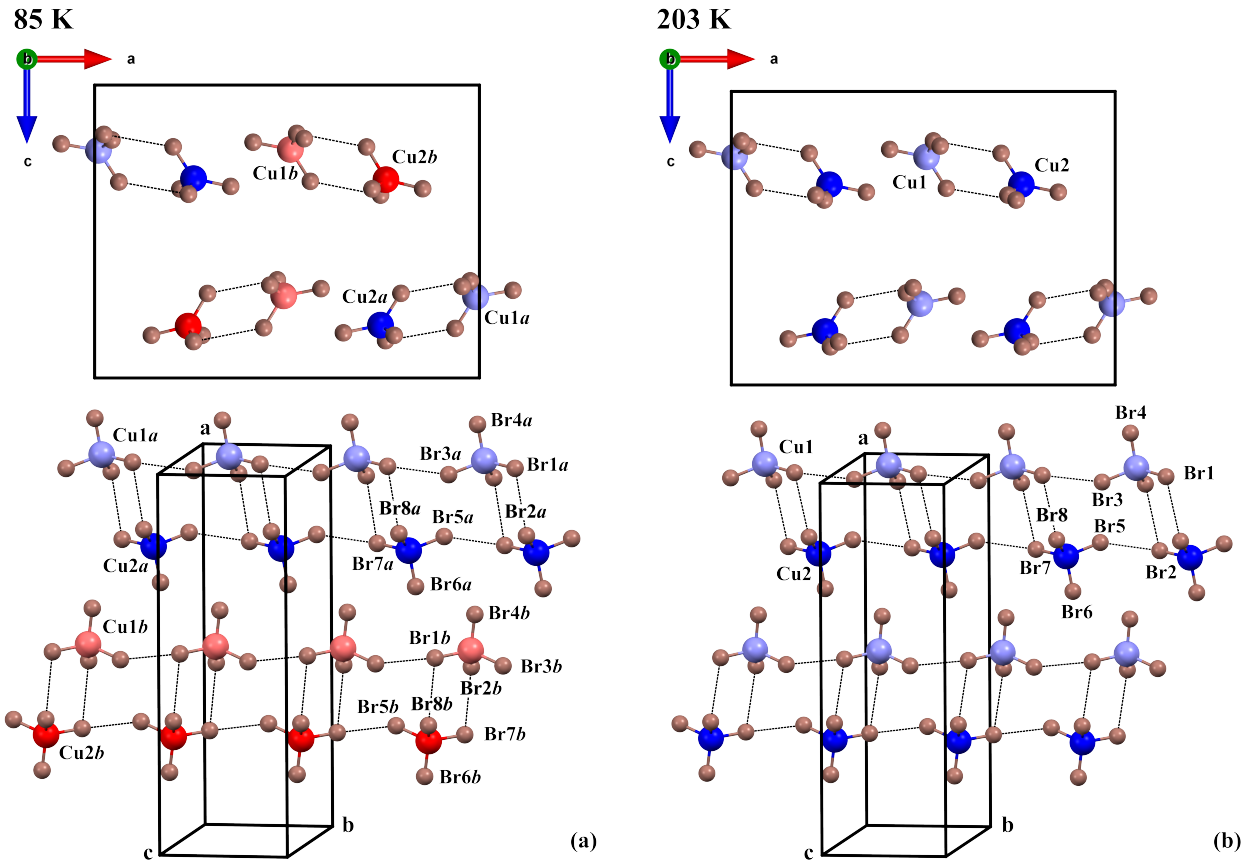

FIG. 1. Key structural elements of Cu-CPA measured at $T = 85$ (a) and 203 K (b). The upper panels show the ladder rungs (dimers) viewed down the b axis. The lower panels provide a perspective view of two of the four ladders in the unit cell. The shortest paths connecting Br^- ions are shown as black lines. The Cu^{2+} ions on opposite side of every ladder rung, marked Cu1 and Cu2, are inequivalent at all temperatures, and below the structural phase transitions there are four inequivalent copper sites (shown as light and dark blue and light and dark red) forming two inequivalent ladders. Because the magnetic interactions depend sensitively on the Cu–Br$\cdots$Br–Cu geometry, we report the different interatomic distances and angles for the 85 K structure in Table II.

datasets were acquired at 95, 105, 115, and 150 K. High-resolution X-ray powder diffraction measurements were performed on the MS beamline [37] at the Swiss Light Source (PSI) on capillary samples using the Mythen III detector. A wavelength of 0.99952 Å, as calibrated with a silicon standard from NIST (SRM 640d), was used for these measurements, while the temperature was controlled using an Oxford Cryosystems Cryostream.

D. Neutron scattering

Additional neutron scattering experiments were performed to confirm the absence of further structural or magnetic phase transitions down to millikelvin temperatures. These used the multiplexing spectrometer CAMEA at the Swiss Spallation Neutron Source (SINQ, PSI) [38, 39] in order to reduce the inelastic background from the sample and sample holder while searching for possible weak magnetic Bragg peaks. The neutron experiments were conducted in a dilution refrigerator attaining temperatures of 30 mK, and the data analyzed with the software package MJOLNIR [40].

III. EXPERIMENTAL RESULTS

A. Specific heat

The specific-heat data from all three measurements, shown in Fig. 2, cover a temperature range (below 200 K) not studied previously. We observe two distinct peaks occurring at temperatures we label as $T^\star = 136$ K and $T^{\mathrm{mono}} = 113$ K in hydrogenated Cu-CPA, with the corresponding peaks for deuterated Cu-CPA appearing over a slightly narrower range. We defer to Secs. III B 1 and III B 2 the explanation of how these two peaks are related to two structural phase transitions.

This observation is unexpected, as to date it had been assumed that the low-temperature structure is achieved below the structural phase transition measured at $T_{2a} = 260$ K [36, 41]. Thus we performed multiple heating and cooling cycles on both the hydrogenated and deuterated compounds in order to confirm that both phase transitions are reversible, reproducible, and independent of the measurement history. Neither phase transition is affected by magnetic fields up to 7 T, further reinforcing the deduction that both are of structural nature.

Although the transitions are sample-independent, they do exhibit an isotope effect (Fig. 2, inset). Compared to

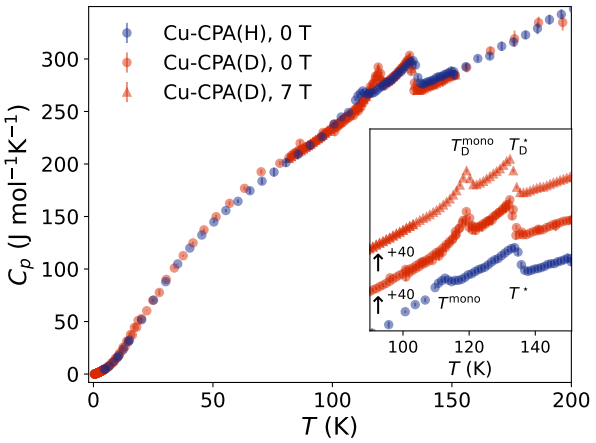

FIG. 2. Specific heat (C_p) as a function of temperature (T), measured for deuterated Cu-CPA samples at ZF (red, circles) and under a magnetic field of 7 T (red, triangles), and for one hydrogenated Cu-CPA sample at ZF (blue, circles). The two peaks at 119 and 132 K for deuterated Cu-CPA, and at 113 and 136 K for hydrogenated Cu-CPA, indicate previously unreported structural phase transitions. Inset: detail of the two phase transitions; the data are displayed with a relative vertical offset. $T^{\rm mono}$ labels the orthorhombic-to-monoclinic transition, whereas $T^\star$ corresponds to the ordering of the organic group.

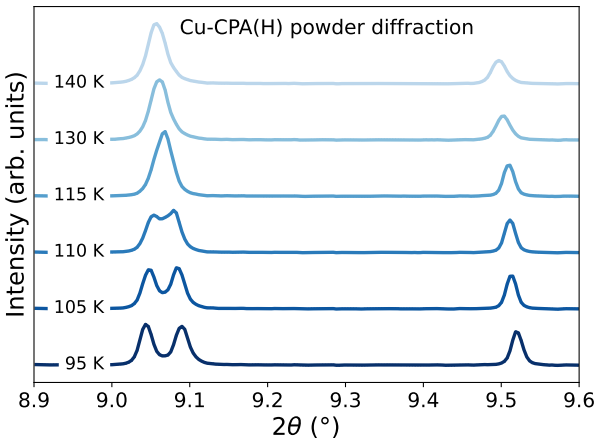

FIG. 3. X-ray powder diffraction patterns obtained for hydrogenated Cu-CPA on lowering the temperature. The splitting of the peak at $2\theta = 9.08°$ between 115 and 110 K indicates a lifting of the degeneracy between the Bragg peaks $(2,1,-1)$ and $(2,1,1)$. This is a signature of the transition into a monoclinic crystal structure, consistent with $T^{\rm mono}$ in Fig. 2. The peak at $2\theta = 9.51°$, corresponding to the Bragg peak $(4,0,0)$, is nondegenerate.

the hydrogenated version of the crystals, the specific-heat peaks in the deuterated samples appear at the slightly different temperatures $T_{\rm D}^\star = 132$ K and $T_{\rm D}^{\rm mono} = 119$ K. Such a change in transition temperatures is a common occurrence in metal-organic systems [42, 43], arising due to the change in donor-acceptor distance within the hydrogen bonds.

Below 100 K, the specific heat varies smoothly down to our lowest measured temperature of 360 mK (Fig. 2). This is consistent with the magnetically disordered ground state expected in a two-leg quantum spin ladder, which is also suggested by measurements of the magnetic susceptibility down to 2 K performed in Ref. [36]. Our neutron scattering measurements further confirmed the absence of any magnetic peaks down to 30 mK.

B. Crystal Structure

We analyzed the crystal structure of Cu-CPA through the two phase transitions by thorough X-ray and neutron scattering experiments. First we confirmed the previously known phase transition at $T_{2a} = 260$ K and refined the crystal structure at 203 K, following Ref. [36]. This structure has orthorhombic space group $Pna2_1$ with lattice parameters $a = 23.9927(6)$ Å, $b = 8.0894(6)$ Å, $c = 18.3449(6)$ Å, and is shown in Fig. 1(b). We adopt it as a frame of reference for the remainder of our discussion. We then solved and refined the crystal structure of Cu-CPA at 85 K, finding the results displayed in Fig. 1(a) and summarized in App. A. We now concentrate on the low-temperature regime ($T \leq 140$ K) in order to relate the specific-heat peaks to two structural phase transitions.

1. *Monoclinic transition*

Figure 3 shows temperature-dependent data from powder X-ray diffraction performed on hydrogenated Cu-CPA. At high temperatures, the peaks at $2\theta = 9.08°$ and $2\theta = 9.51°$ correspond respectively to the Bragg peaks $[(2,1,-1), (2,1,1)]$ and $(4,0,0)$, as defined in the orthorhombic crystal structure of the system at 203 K. The splitting of the peak at $2\theta = 9.08°$ below 115 K corresponds to a structural phase transition and a decrease of crystal symmetry from orthorhombic to monoclinic. At this transition, the crystallographic angle γ changes from 90° to 90.3°, which is manifested most clearly in a splitting of mixed Bragg peaks that involve the c direction, such as $(2,1,-1)$ and $(2,1,1)$. Above 115 K, these peaks coincide by symmetry, but the structural phase transition leads to a change of space group from $Pna2_1$ to $P112_1$ and a lifting of degeneracies. Because the onset temperature of the splitting is consistent with the lower-temperature peak observed in our specific-heat measurements, we assign this phase transition to $T^{\rm mono}$. It is this orthorhombic-to-monoclinic transition that causes the ladders to become pairwise structurally inequivalent [Fig. 1(a)].

Finally, we state that this transition is continuous, as shown by the temperature dependence of the monoclinic angle γ, reported in Table IV.

2. *Order-disorder transition*

We now turn to the phase transition taking place at $T^\star$. Our structural measurements revealed no additional lowering of symmetry at this temperature. We describe, instead, the atomic reorganization at $T^\star$ as an order-disorder transition. Indeed, the authors of Ref. [36] demonstrated the presence of disorder in the organic

cations. A full structural dataset was therefore taken by X-ray diffraction on a deuterated single crystal of Cu-CPA at 125 K (i.e. directly below $T^\star$ but still above $T^{\rm mono}$). At variance from the 203 K dataset, collected on the same crystal, upon refinement of this 125 K dataset, we did not have to include any disorder during refinement of the organic cations, confirming that the $T^\star$ transition is of order-disorder type.

3. *Relevant pathways between magnetic ions*

The magnetic interactions in insulating materials result from extended superexchange processes on the pathways between magnetic ions. Because they depend on the overlap of electronic orbitals along these pathways, they have a strong and highly nonlinear dependence on the interatomic separations ("bond lengths") and on the angles between bonds [44, 45]. To tabulate all the information required to estimate the relevant magnetic interactions, in Table I we first report the Cu–Br bond lengths and angles within the $CuBr_4^{2-}$ anions. The primary differences between the 85 K structure and the 203 K structure reported previously are a consequence of the orthorhombic-to-monoclinic transition, which leads to a minor deformation of the $CuBr_4$ tetrahedra [Fig. 1(a)]. This deformation creates four inequivalent Cu sites in the low-temperature structure, compared to two above $T^{\rm mono}$.

To address the Cu–Cu pathways, in Table II we show the Br$\cdots$Br distances, Cu–Br$\cdots$Br and Br$\cdots$Br–Cu angles, and the dihedral angle τ for each of the inequivalent ladders. We denote sites in the two inequivalent ladders with the subscripts a and b. The shortest Br$\cdots$Br distances correspond to the ladder legs, and are shortened by at most 1.7% on passing from the 203 K structure to the 85 K structure, while the Cu–Br$\cdots$Br angles change by at most 0.7%. A more pronounced change is found on the ladder rungs (second group of four in Table II), where some bond angles decrease by up to 4% in both ladder a and ladder b. On the intraladder, diagonal pathway (third group of four), the halogen-bond length increases in both inequivalent ladders, by 1% to 4%. If one inquires about the biggest change between the two inequivalent ladders, this is found in the halogen-bond length on the rungs, which increases by up to 1.5% on ladder a while decreasing by up to 1.8% on ladder b.

TABLE I. Cu–Br bond lengths [Å] and Br–Cu–Br angles [deg] in the Cu-CPA structure at 85 K and at 203 K. The atomic site notation is that of Fig. 1.

Bonds	$T = 85$ K	$T = 203$ K
Cu_{1a}–Br_{1a}	2.368(4)	2.358(2)
Cu_{1b}–Br_{1b}	2.367(4)	
Cu_{1a}–Br_{2a}	2.370(3)	2.359(2)
Cu_{1b}–Br_{2b}	2.370(4)	
Cu_{1a}–Br_{3a}	2.399(3)	2.398(2)
Cu_{1b}–Br_{3b}	2.398(3)	
Cu_{1a}–Br_{4a}	2.388(3)	2.378(2)
Cu_{1b}–Br_{4b}	2.384(4)	
Cu_{2a}–Br_{5a}	2.404(3)	2.388(2)
Cu_{2b}–Br_{5b}	2.399(3)	
Cu_{2a}–Br_{6a}	2.392(3)	2.389(2)
Cu_{2b}–Br_{6b}	2.394(3)	
Cu_{2a}–Br_{7a}	2.365(3)	2.360(2)
Cu_{2b}–Br_{7b}	2.363(3)	
Cu_{2a}–Br_{8a}	2.376(4)	2.368(2)
Cu_{2b}–Br_{8b}	2.380(3)	
Br_{1a}–Cu_{1a}–Br_{2a}	99.54(12)	99.06(8)
Br_{1b}–Cu_{1b}–Br_{2b}	99.18(13)	
Br_{1a}–Cu_{1a}–Br_{3a}	129.67(12)	127.50(10)
Br_{1b}–Cu_{1b}–Br_{3b}	128.05(14)	
Br_{1a}–Cu_{1a}–Br_{4a}	101.20(12)	102.08(9)
Br_{1b}–Cu_{1b}–Br_{4b}	102.13(15)	
Br_{2a}–Cu_{1a}–Br_{3a}	97.87(11)	98.45(8)
Br_{2b}–Cu_{1b}–Br_{3b}	99.13(12)	
Br_{2a}–Cu_{1a}–Br_{4a}	134.10(12)	133.61(10)
Br_{2b}–Cu_{1b}–Br_{4b}	132.15(14)	
Br_{3a}–Cu_{1a}–Br_{4a}	99.52(12)	100.48(8)
Br_{3b}–Cu_{1b}–Br_{4b}	100.44(13)	
Br_{5a}–Cu_{2a}–Br_{6a}	98.50(12)	99.23(7)
Br_{5b}–Cu_{2b}–Br_{6b}	99.10(12)	
Br_{5a}–Cu_{2a}–Br_{7a}	130.60(12)	129.75(9)
Br_{5b}–Cu_{2b}–Br_{7b}	131.28(12)	
Br_{5a}–Cu_{2a}–Br_{8a}	98.48(12)	98.62(7)
Br_{5b}–Cu_{2b}–Br_{8b}	97.84(12)	
Br_{6a}–Cu_{2a}–Br_{7a}	100.31(12)	100.87(8)
Br_{6b}–Cu_{2b}–Br_{7b}	99.98(12)	
Br_{6a}–Cu_{2a}–Br_{8a}	135.72(13)	134.83(10)
Br_{6b}–Cu_{2b}–Br_{8b}	134.66(12)	
Br_{7a}–Cu_{2a}–Br_{8a}	98.94(12)	98.81(7)
Br_{7b}–Cu_{2b}–Br_{8b}	99.65(12)	

IV. DISCUSSION

Interpretation of the phenomena observed in quantum magnetic materials depends crucially on the availability of realistic model Hamiltonians. For this the underlying crystal structure provides essential insight into the symmetry, number, and relative strengths of the relevant interaction parameters. For $(C_5H_9NH_3)_2CuBr_4$ we have found that the two-parameter, strong-leg ladder Hamiltonian assumed previously is in fact incomplete. The discovery of two inequivalent ladders at low temperatures requires that existing measurements be interpreted in a new light and establishes the foundation for future spectroscopic studies of this model two-ladder material.

First, we address the implications of the low-temperature crystal structure for the magnetic interaction parameters. In an ideal two-leg ladder one expects only two interaction parameters, $J_{\rm leg}$ and $J_{\rm rung}$. Here we note that in Cu-CPA even the 203 K structure may have two additional complications due to the fact that the two Cu atoms are inequivalent. First, the two leg bonds may not be identical. Second, the rungs possess no center of inversion symmetry and hence may have a finite DM interaction; a rung DM term can cause significant modification of the magnetic properties of a ladder [33], for which it is also more effective than a leg DM term. At low temperatures, the number of interaction parameters required to describe the system is doubled. Because the Cu–Br$\cdots$Br–Cu pathways differ slightly in length and angle for each of the four inequivalent copper sites, we

TABLE II. Interatomic distances and angles involving the Br···Br bonds at $T = 85$ K. τ is the dihedral angle. The data separate by distance into three groups of four and one group of two, which correspond to pathways composing the leg, rung, diagonal, and interladder interactions. The different interaction parameters appearing in a minimal Heisenberg spin Hamiltonian (Fig. 4) are given in the "Interaction" column.

Atoms	$T = 85$ K				Interaction	$T = 203$ K			
	$d_{\mathrm{Br-Br}}$ [Å]	$\theta_{\mathrm{Cu-Br\cdots Br}}$ [°]	$\theta_{\mathrm{Br\cdots Br-Cu}}$ [°]	τ [°]		$d_{\mathrm{Br-Br}}$ [Å]	$\theta_{\mathrm{Cu-Br\cdots Br}}$ [°]	$\theta_{\mathrm{Br\cdots Br-Cu}}$ [°]	τ [°]
Cu_{1a}–$Br_{1a}\cdots Br_{3a}$–Cu_{1a}	3.856(3)	149.6(1)	149.8(1)	65.2(3)	$J_{\mathrm{leg},1a}$	3.893(3)	149.8(3)	150.1(1)	55.9(5)
Cu_{1b}–$Br_{1b}\cdots Br_{3b}$–Cu_{1b}	3.871(3)	150.0(1)	149.6(1)	58.8(4)	$J_{\mathrm{leg},1b}$				
Cu_{2a}–$Br_{5a}\cdots Br_{7a}$–Cu_{2a}	3.841(3)	148.4(1)	151.5(1)	66.9(3)	$J_{\mathrm{leg},2a}$	3.881(3)	148.8(1)	151.0(2)	64.3(5)
Cu_{2b}–$Br_{5b}\cdots Br_{7b}$–Cu_{2b}	3.849(3)	149.8(1)	149.2(1)	71.4(3)	$J_{\mathrm{leg},2b}$				
Cu_{1a}–$Br_{1a}\cdots Br_{8a}$–Cu_{2a}	4.350(4)	100.7(1)	134.5(1)	65.8(2)	$J_{\mathrm{rung},a}$	4.396(4)	105.3(1)	133.8(2)	62.5(3)
Cu_{1b}–$Br_{1b}\cdots Br_{8b}$–Cu_{2b}	4.526(5)	101.3(1)	131.5(1)	66.4(2)	$J_{\mathrm{rung},b}$				
Cu_{1a}–$Br_{2a}\cdots Br_{7a}$–Cu_{2a}	4.408(3)	133.3(1)	99.9(1)	66.9(2)	$J_{\mathrm{rung},a}$	4.519(4)	132.1(2)	103.2(1)	63.4(2)
Cu_{1b}–$Br_{2b}\cdots Br_{7b}$–Cu_{2b}	4.534(3)	133.2(1)	99.9(1)	66.9(2)	$J_{\mathrm{rung},b}$				
Cu_{1a}–$Br_{2a}\cdots Br_{5a}$–Cu_{2a}	4.960(3)	114.1(1)	145.1(1)	22.7(2)	$J_{\mathrm{diag},a}$	4.930(4)	114.6(1)	143.6(1)	27.1(4)
Cu_{1b}–$Br_{2b}\cdots Br_{5b}$–Cu_{2b}	5.078(3)	113.3(1)	146.3(1)	28.4(2)	$J_{\mathrm{diag},b}$				
Cu_{1a}–$Br_{3a}\cdots Br_{8a}$–Cu_{2a}	4.953(3)	145.8(1)	113.8(1)	23.2(2)	$J_{\mathrm{diag},a}$	4.919(4)	143.8(1)	114.6(1)	24.6(4)
Cu_{1b}–$Br_{3b}\cdots Br_{8b}$–Cu_{2b}	5.161(3)	144.2(1)	112.7(1)	25.3(2)	$J_{\mathrm{diag},b}$				
Cu_{1a}–$Br_{4a}\cdots Br_{6b}$–Cu_{2b}	5.080(4)	107.2(1)	90.9(1)	173.4(1)	$J_{\mathrm{interladder},1}$	5.146(5)	94.3(1)	107.0(1)	170.5(3)
Cu_{1b}–$Br_{4b}\cdots Br_{6a}$–Cu_{2a}	4.956(4)	105.7(1)	92.5(1)	170.0(1)	$J_{\mathrm{interladder},2}$				

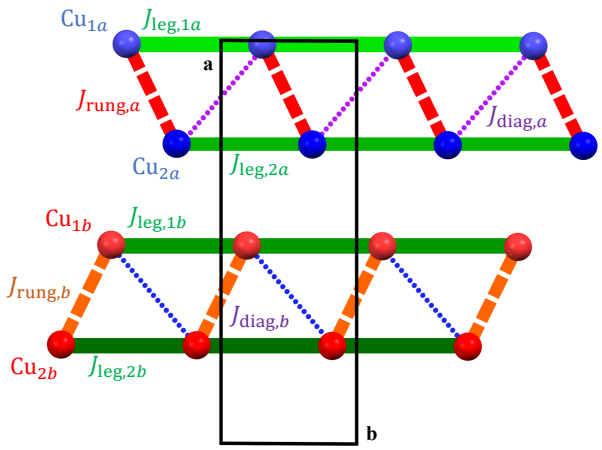

FIG. 4. Schematic representation of the interaction parameters expected on the basis of the inequivalent atomic pathways in the two ladders of Cu-CPA (Table II). The four inequivalent leg interactions, $J_{\mathrm{leg},1a}$, $J_{\mathrm{leg},2a}$, $J_{\mathrm{leg},1b}$, and $J_{\mathrm{leg},2b}$, are shown as green, solid lines. The two inequivalent rung interactions, $J_{\mathrm{rung},a}$ and $J_{\mathrm{rung},b}$, are shown respectively as dashed red and orange lines. The diagonal interactions, $J_{\mathrm{diag},a}$ and $J_{\mathrm{diag},b}$ are depicted respectively as purple and blue dotted lines. A possible small interladder interaction is not represented.

expect four different values for the leg interactions in Cu-CPA (Table II, first group of four), as depicted in Fig. 4. Because the geometries of all four pathways are rather similar, one may anticipate that the corresponding interaction parameters should be comparable in strength, but the extreme sensitivity of superexchange interactions to bond lengths and angles means that our results certainly do not exclude differences in the range of 10s of percent.

Turning to the rung pathways (Table II, second group of four), it is clear that Cu-CPA features two sets of rung interaction parameters, which, from their bond lengths and angles, will be more different from one another. Thus Cu-CPA could offer a superposition of two strong-leg ladders with significantly different leg-to-rung coupling ratios. All further Br···Br bonds are considerably longer again (close to 5 Å), suggesting very small interactions. These fall into two groups, the first corresponding to one diagonal intraladder interaction per inequivalent ladder (Table II, third group of four); at lowest order, a diagonal term in a two-leg ladder is an interrung interaction whose effective sign is opposite to J_{leg}, and in Cu-CPA should be a negligible alteration to the effects of the four J_{leg} bonds. The second group (Table II, final pair) corresponds to interladder bonds, which even if tiny would dictate the onset of three-dimensional magnetic order in applied magnetic fields above the ladder gap, or gaps [12, 15].

We now address previously reported magnetic measurements. The authors of Ref. [36] were able to reproduce their observed magnetic susceptibility using the minimal model of an ideal (two-parameter) quantum spin ladder, deducing a $J_{\mathrm{leg}}/J_{\mathrm{rung}}$ ratio in the strong-leg regime. We have remeasured the susceptibility and obtained fully consistent results; no signature of the two-ladder nature of Cu-CPA can be found in these datasets. Quite generally, the magnetic susceptibility, and indeed most other bulk probes, provide very general information from which it is possible to infer only a small number of independent energy scales. This is particularly true in Cu-CPA, where the rather weak interactions ($J_{\mathrm{leg}} = 11.6$ K and $J_{\mathrm{rung}} = 5.5$ K) mandate dilution temperatures in order to extract the spin gap independently. In the particular case of a two-ladder system, one may expect from bulk measurements to determine at best average values for the couplings in the two ladders. Thus detailed spectroscopic studies, preferably in combination with *ab initio* calculations, are required for the determination of the multiple interaction parameters in Fig. 4.

We turn next to measurements of the magnetization. Although the results of Ref. [36] were obtained at a temperature below the estimated spin gap, and show the

expected trend of a monotonic increase until saturation, they show neither a sharp onset at low fields nor the approach to saturation of a ladder model. With the insight that the system possesses two inequivalent ladders, the slow onset of the magnetization may be explained by the presence of two spin gaps. Similarly, the mismatch in near-saturation behavior could be a result of two different ladders with distinct saturation fields. Finally, it has been proposed that subtle tendencies toward the formation of plateaus in the magnetization could appear due to the field-induced reorientation of the $CuBr_4^{2-}$ anions [41]. While this physics may occur, a detailed understanding of the spin excitation spectrum is required in order to exclude simpler scenarios. In the light of our structural findings, a sub-100 mK magnetization measurement should be combined with neutron spectroscopy to elucidate the magnetic behavior of Cu-CPA.

An important implication of the rather strong isotope effect we observe on the phase-transition temperatures is the softness of the structure. As a result, Cu-CPA is an excellent candidate for studying pressure-induced quantum phenomena [46]. In contrast to previous studies of pressure effects in dimerized quantum magnets, which concentrated on strong-dimer materials with well defined triplon or magnon excitations [47–49], Cu-CPA is thought to realize a model displaying the fingerprints of weakly confined spinons, and hence offers different possibilities for quantum phase transitions and the evolution of spin excitations. Finally, it remains to be determined whether the excitations of the two inequivalent ladders may have an appreciable interaction term, which could then manifest itself in unconventional behavior either under ambient conditions or under applied external fields or pressures.

V. CONCLUSIONS

In summary, our studies reveal two previously unknown structural phase transitions in the metal-organic quantum magnet $(C_5H_9NH_3)_2CuBr_4$. By characterizing the low-temperature structure we establish Cu-CPA as an experimental realization of a two-ladder model and hence as a promising material in which to search for additional magnetic excitations in the strong-leg regime.

ACKNOWLEDGMENTS

We thank D. Le and R. Valenti for helpful discussions. This project was supported by the Horizon 2020 research and innovation program of the European Union under the Marie Skłodowska-Curie Grant (Agreement No. 884104, PSI-FELLOW-III-3i). We acknowledge in addition the support of the Chalmers X-Ray and Neutron Initiatives (CHANS) and the Swedish Research Council (VR) through a Starting Grant (No. Dnr. 2017-05078) and through a Grant (No. 2022-06217) and the Foundation Blanceflor 2023 fellow scholarship and through the Area of Advance-Material Sciences of Chalmers University of Technology. We are grateful to the Paul Scherrer Institute for the allocation of neutron beam time on CAMEA at SINQ (under Project No. 20212923).

Appendix A: Structural properties

We summarize the properties of $(C_5H_9NH_3)_2CuBr_4$ and $(C_5D_9ND_3)_2CuBr_4$ in Table III. We draw attention to the mass difference, which is important for an accurate comparison of the specific-heat measurements.

TABLE III. Structural properties of the hydrogenated (obtained from powder X-ray diffraction) and deuterated (obtained from single-crystal X-ray diffraction) compounds at 95 and 85 K, respectively.

chemical formula	$C_{10}H_{24}Br_4CuN_2$	$C_{10}D_{24}Br_4CuN_2$
f.w. [g/mol]	555.49	579.29
T [K]	95(2)	85(2)
cryst. system	monoclinic	monoclinic
space group	$P112_1$	$P112_1$
a [Å]	23.9649	23.9549(16)
b [Å]	8.0765	8.0759(6)
c [Å]	18.2819	18.2733(13)
α [°]	90	90
β [°]	90	90
γ [°]	90.35	90.30(1)
V [Å^3]	3538.44	3535.06

Appendix B: Lattice evolution

In this appendix, we show the temperature dependence of the lattice parameters a, b and c as well as the monoclinic angle γ (the two angles α and β remain 90.00°). These values were refined from the X-ray powder diffraction patterns obtained for hydrogenated Cu-CPA, as reported in Fig. 3.

The reported change of monoclinic angle γ shows that this phase transition is a continuous process, saturating around $\gamma \simeq 90.3°$.

TABLE IV. Structure and lattice evolution refined from X-ray powder diffraction of hydrogenated Cu-CPA. .

T [K]	a [Å]	b [Å]	c [Å]	γ [°]
155	24.0419	8.0763	18.3965	90
150	24.0392	8.0763	18.3850	90
145	24.0259	8.0719	18.3944	90
140	24.0198	8.0712	18.3890	90
135	24.0100	8.0695	18.3862	90
130	24.0071	8.0700	18.3725	90
125	24.0002	8.0697	18.3655	90
120	23.9984	8.0705	18.3495	90
110	23.9872	8.0687	18.3417	90.21
105	23.9826	8.0700	18.3277	90.29
100	23.9754	8.0727	18.3053	90.34
95	23.9649	8.0765	18.2819	90.35

[1] E. Dagotto and T. M. Rice, Surprises on the Way from One- to Two-Dimensional Quantum Magnets: The Ladder Materials, Science **271**, 618 (1996).

[2] S. R. White, R. M. Noack, and D. J. Scalapino, Resonating Valence Bond Theory of Coupled Heisenberg Chains, Phys. Rev. Lett. **73**, 886 (1994).

[3] D. Schmidiger, S. Mühlbauer, A. Zheludev, P. Bouillot, T. Giamarchi, C. Kollath, G. Ehlers, and A. M. Tsvelik, Symmetric and asymmetric excitations of a strong-leg quantum spin ladder, Phys. Rev. B **88**, 094411 (2013).

[4] T. Giamarchi and A. M. Tsvelik, Coupled ladders in a magnetic field, Phys. Rev. B **59**, 11398 (1999).

[5] Z. Hiroi, M. Azuma, M. Takano, and Y. Bando, A new homologous series $Sr_{n-1}Cu_{n+1}O_{2n}$ found in the SrO-CuO system treated under high pressure, J. Solid State Chem. **95**, 230 (1991).

[6] M. Azuma, Z. Hiroi, M. Takano, K. Ishida, and Y. Kitaoka, Observation of a Spin Gap in $SrCu_2O_3$ Comprising Spin-1/2 Quasi-1D Two-Leg Ladders, Phys. Rev. Lett. **73**, 3463 (1994).

[7] K. Ishida, Y. Kitaoka, K. Asayama, M. Azuma, Z. Hiroi, and M. Takano, Spin Gap Behavior in Ladder-Type of Quasi-One-Dimensional Spin $S = 1/2$ System $SrCu_2O_3$, Phys. Rev. Lett. **63**, 3222 (1994).

[8] K. Kojima, A. Keren, G. M. Luke, B. Nachumi, W. D. Wu, Y. J. Uemura, M. Azuma, and M. Takano, Magnetic Behavior of the 2-Leg and 3-Leg Spin Ladder Cuprates $Sr_{n-1}Cu_{n+1}O_{2n}$, Phys. Rev. Lett. **74**, 2812 (1995).

[9] Z. Hiroi and M. Takano, Absence of superconductivity in the doped antiferromagnetic spin-ladder compound $(La,Sr)CuO_{2.5}$, Nature **377**, 41 (1995).

[10] H. Mayaffre, P. Auban-Senzier, M. Nardone, D. Jérome, D. Poilblanc, C. Bourbonnais, U. Ammerahl, G. Dhalenne, and A. Revcolevschi, Absence of a Spin Gap in the Superconducting Ladder Compound $Sr_2Ca_{12}Cu_{24}O_{41}$, Science **279**, 345 (1998).

[11] R. S. Eccleston, M. Uehara, J. Akimitsu, H. Eisaki, N. Motoyama, and S. Uchida, Spin Dynamics of the Spin-Ladder Dimer-Chain Material $Sr_{14}Cu_{24}O_{41}$, Phys. Rev. Lett. **81**, 1702 (1998).

[12] M. Klanjšek, H. Mayaffre, C. Berthier, M. Horvatić, B. Chiari, O. Piovesana, P. Bouillot, C. Kollath, E. Orignac, R. Citro, and T. Giamarchi, Controlling Luttinger Liquid Physics in Spin Ladders under a Magnetic Field, Phys. Rev. Lett. **101**, 137207 (2008).

[13] Ch. Rüegg, K. Kiefer, B. Thielemann, D. F. McMorrow, V. Zapf, B. Normand, M. B. Zvonarev, P. Bouillot, C. Kollath, T. Giamarchi, S. Capponi, D. Poilblanc, D. Biner, and K. W. Krämer, Thermodynamics of the Spin Luttinger Liquid in a Model Ladder Material, Phys. Rev. Lett. **101**, 247202 (2008).

[14] B. Thielemann, Ch. Rüegg, H. M. Rønnow, A. M. Läuchli, J.-S. Caux, B. Normand, D. Biner, K. W. Krämer, H.-U. Güdel, J. Stahn, K. Habicht, K. Kiefer, M. Boehm, D. F. McMorrow, and J. Mesot, Direct Observation of Magnon Fractionalization in the Quantum Spin Ladder, Phys. Rev. Lett. **102**, 107204 (2009).

[15] B. Thielemann, Ch. Rüegg, K. Kiefer, H. M. Rønnow, B. Normand, P. Bouillot, C. Kollath, E. Orignac, R. Citro, T. Giamarchi, A. M. Läuchli, D. Biner, K. W. Krämer, F. Wolff-Fabris, V. S. Zapf, M. Jaime, J. Stahn, N. B. Christensen, B. Grenier, D. F. McMorrow, and J. Mesot, Field-controlled magnetic order in the quantum spin-ladder system $(Hpip)_2CuBr_4$, Phys. Rev. B **79**, 020408 (2009).

[16] P. Bouillot, C. Kollath, A. M. Läuchli, M. Zvonarev, B. Thielemann, Ch. Rüegg, E. Orignac, R. Citro, M. Klanjšek, C. Berthier, M. Horvatić, and T. Giamarchi, Statics and dynamics of weakly coupled antiferromagnetic spin-$\frac{1}{2}$ ladders in a magnetic field, Phys. Rev. B **83**, 054407 (2011).

[17] M. Windt, M. Grüninger, T. Nunner, C. Knetter, K. P. Schmidt, G. S. Uhrig, T. Kopp, A. Freimuth, U. Ammerahl, B. Büchner, and A. Revcolevschi, Observation of Two-Magnon Bound States in the Two-Leg Ladders of $(Ca,La)_{14}Cu_{24}O_{41}$, Phys. Rev. Lett. **87**, 127002 (2001).

[18] D. Schmidiger, P. Bouillot, S. Mühlbauer, S. Gvasaliya, C. Kollath, T. Giamarchi, and A. Zheludev, Spectral and Thermodynamic Properties of a Strong-Leg Quantum Spin Ladder, Phys. Rev. Lett. **108**, 167201 (2012).

[19] S. Ward, M. Mena, P. Bouillot, C. Kollath, T. Giamarchi, K. P. Schmidt, B. Normand, K. W. Krämer, D. Biner, R. Bewley, T. Guidi, M. Boehm, D. F. McMorrow, and Ch. Rüegg, Bound States and Field-Polarized Haldane Modes in a Quantum Spin Ladder, Phys. Rev. Lett. **118**, 177202 (2017).

[20] Y. Xian, Rigorous results on a first-order phase transition in antiferromagnetic spin-1/2 coupled chains, Phys. Rev. B **52**, 12485 (1995).

[21] A. Honecker, S. Wessel, R. Kerkdyk, T. Pruschke, F. Mila, and B. Normand, Thermodynamic properties of highly frustrated quantum spin ladders: Influence of many-particle bound states, Phys. Rev. B **93**, 054408 (2016).

[22] A. Honecker, F. Mila, and B. Normand, Multi-triplet bound states and finite-temperature dynamics in highly frustrated quantum spin ladders, Phys. Rev. B **94**, 094402 (2016).

[23] A. Shapiro, C. P. Landee, M. M. Turnbull, J. Jornet, M. Deumal, J. J. Novoa, M. A. Robb, and W. Lewis, Synthesis, Structure, and Magnetic Properties of an Antiferromagnetic Spin-Ladder Complex: Bis(2,3-dimethylpyridinium) Tetrabromocuprate, J. Am. Chem. Soc. **129**, 952 (2007).

[24] T. Hong, Y. H. Kim, C. Hotta, Y. Takano, G. Tremelling, M. M. Turnbull, C. P. Landee, H.-J. Kang, N. B. Christensen, K. Lefmann, K. P. Schmidt, G. S. Uhrig, and C. Broholm, Field-Induced Tomonaga-Luttinger Liquid Phase of a Two-Leg Spin-1/2 Ladder with Strong Leg Interactions, Phys. Rev. Lett. **105**, 137207 (2010).

[25] D. Schmidiger, S. Muehlbauer, S. N. Gvasaliya, T. Yankova, and A. Zheludev, Long-lived magnons throughout the Brillouin zone of the strong-leg spin ladder $(C_7H_{10}N)_2CuBr_4$, Phys. Rev. B **84**, 144421 (2011).

[26] D. Schmidiger, P. Bouillot, T. Guidi, R. Bewley, C. Kollath, T. Giamarchi, and A. Zheludev, Spectrum of a magnetized strong-leg quantum spin ladder, Phys. Rev. Lett. **111**, 107202 (2013).

[27] K. Ninios, T. Hong, T. Manabe, C. Hotta, S. N. Herringer, M. M. Turnbull, C. P. Landee, Y. Takano, and H. B. Chan, Wilson Ratio of a Tomonaga-Luttinger Liquid in a Spin-1/2 Heisenberg Ladder, Phys. Rev. Lett. **108**, 097201 (2012).

[28] M. Jeong, H. Mayaffre, C. Berthier, D. Schmidiger, A. Zheludev, and M. Horvatić, Attractive Tomonaga-Luttinger Liquid in a Quantum Spin Ladder, Phys. Rev. Lett. **111**, 106404 (2013).

[29] K. Y. Povarov, D. Schmidiger, N. Reynolds, R. Bewley, and A. Zheludev, Scaling of temporal correlations in an attractive Tomonaga-Luttinger spin liquid, Phys. Rev. B **91**, 020406(R) (2015).

[30] M. Jeong, D. Schmidiger, H. Mayaffre, M. Klanjšek, C. Berthier, W. Knafo, G. Ballon, B. Vignolle, S. Krämer, A. Zheludev, and M. Horvatić, Dichotomy between Attractive and Repulsive Tomonaga-Luttinger Liquids in Spin Ladders, Phys. Rev. Lett. **117**, 106402 (2016).

[31] D. Schmidiger, K. Povarov, S. Galeski, N. Reynolds, R. Bewley, T. Guidi, J. Ollivier, and A. Zheludev, Emergent Interacting Spin Islands in a Depleted Strong-Leg Heisenberg Ladder, Phys. Rev. Lett. **116**, 257203 (2016).

[32] M. Jeong, H. Mayaffre, C. Berthier, D. Schmidiger, A. Zheludev, and M. Horvatić, Magnetic-Order Crossover in Coupled Spin Ladders, Phys. Rev. Lett. **118**, 167206 (2017).

[33] K. Penc, J.-B. Fouet, S. Miyahara, O. Tchernyshyov, and F. Mila, Ising Phases of Heisenberg Ladders in a Magnetic Field, Phys. Rev. Lett. **99**, 117201 (2007).

[34] F. Michaud, T. Coletta, S. R. Manmana, J.-D. Picon, and F. Mila, Frustration-induced plateaus in $S \geq \frac{1}{2}$ Heisenberg spin ladders, Phys. Rev. B **81**, 014407 (2010).

[35] A. Weichselbaum, W. Yin, and A. M. Tsvelik, Dimerization and spin decoupling in a two-leg Heisenberg ladder with frustrated trimer rungs, Phys. Rev. B **103**, 125120 (2021).

[36] R. D. Willett, C. Galeriu, C. P. Landee, M. M. Turnbull, and B. Twamley, Structure and magnetism of a spin ladder system: $(C_5H_9NH_3)_2CuBr_4$, Inorg. Chem. **43**, 3804 (2004).

[37] P. R. Willmott, D. Meister, S. J. Leake, M. Lange, A. Bergamaschi, M. Böge, M. Calvi, C. Cancellieri, N. Casati, A. Cervellino, Q. Chen, C. David, U. Flechsig, F. Gozzo, B. Henrich, S. Jäggi-Spielmann, B. Jakob, I. Kalichava, P. Karvinen, J. Krempasky, A. Lüdeke, R. Lüscher, S. Maag, C. Quitmann, M. L. Reinle-Schmitt, T. Schmidt, B. Schmitt, A. Streun, I. Vartiainen, M. Vitins, X. Wang, and R. Wullschleger, The Materials Science beamline upgrade at the Swiss Light Source, J. Synchrotron Rad. **20**, 667 (2013).

[38] F. Groitl, D. Graf, J. O. Birk, M. Markó, M. Bartkowiak, U. Filges, C. Niedermayer, Ch. Rüegg, and H. M. Rønnow, CAMEA — A novel multiplexing analyzer for neutron spectroscopy, Rev. Sci. Instrum. **87**, 035109 (2016).

[39] J. Lass, H. Jacobsen, K. M. L. Krighaar, D. Graf, F. Groitl, F. Herzog, M. Yamada, C. Kägi, R. A. Müller, R. Bürge, M. Schild, M. S. Lehmann, A. Bollhalder, P. Keller, M. Bartkowiak, U. Filges, U. Greuter, G. Theidel, H. M. Rønnow, C. Niedermayer, and D. G. Mazzone, Commissioning of the novel Continuous Angle Multi-energy Analysis spectrometer at the Paul Scherrer Institut, Rev. Sci. Instrum. **94**, 023302 (2023).

[40] J. Lass, H. Jacobsen, D. Mazzone, and K. Lefmann, MJOLNIR: A software package for multiplexing neutron spectrometers, SoftwareX **12**, 100600 (2020).

[41] J. D. Woodward, J. Choi, J. L. Musfeldt, J. T. Haraldsen, X. Wei, H.-J. Koo, D. Dai, M.-H. Whangbo, C. P. Landee, and M. M. Turnbull, Understanding the color properties of $(C_5H_9NH_3)_2CuBr_4$ in high magnetic fields, Phys. Rev. B **71**, 174416 (2005).

[42] R. E. Wilson, Structure, Phase Transitions, and Isotope Effects in $[(CH_3)_4N]_2PuCl_6$, Inorg. Chem. **54**, 10208 (2015).

[43] C. Shi, X. Zhang, C.-H. Yu, Y.-F. Yao, and W. Zhang, Geometric isotope effect of deuteration in a hydrogen-bonded host–guest crystal, Nat. Commun. **9**, 481 (2018).

[44] M. M. Turnbull, C. P. Landee, and B. M. Wells, Magnetic exchange interactions in tetrabromocuprate compounds, Coord. Chem. Rev. **249**, 2567 (2005).

[45] K. Foyevtsova, I. Opahle, Y.-Z. Zhang, H. O. Jeschke, and R. Valentí, Determination of effective microscopic models for the frustrated antiferromagnets Cs_2CuCl_4 and Cs_2CuBr_4 by density functional methods, Phys. Rev. B **83**, 125126 (2011).

[46] S. Sachdev, Quantum magnetism and criticality, Nat. Phys. **4**, 173 (2008).

[47] Ch. Rüegg, A. Furrer, D. Sheptyakov, T. Strässle, K. W. Krämer, H.-U. Güdel, and L. Mélési, Pressure-Induced Quantum Phase Transition in the Spin-Liquid $TlCuCl_3$, Phys. Rev. Lett. **93**, 257201 (2004).

[48] M. Thede, A. Mannig, M. Månsson, D. Hüvonen, R. Khasanov, E. Morenzoni, and A. Zheludev, Pressure-Induced Quantum Critical and Multicritical Points in a Frustrated Spin Liquid, Phys. Rev. Lett. **112**, 087204 (2014).

[49] S. Bettler, G. Simutis, G. Perren, D. Blosser, S. Gvasaliya, and A. Zheludev, High-pressure Raman study of the quantum magnet $(C_4H_{12}N_2)Cu_2Cl_6$, Phys. Rev. B **96**, 174431 (2017).